Analysis and Quantification of Errors in the Geometric Correction of Satellite Images

Gary E. Ford
Claudio I. Zanelli
Department of Electrical and Computer Engineering, University of California, Davis, CA 95616

ABSTRACT: The quantitative use of remote sensing satellite images in many applications requires that the geometric distortion inherent in these images be corrected, or rectified, to a desired map projection. The most widely used technique relies on ground control points to empirically determine a mathematical coordinate transformation to correct the geometry. In this paper, using the method of least squares, expressions for the accuracy of the geometric transformation and of the rectification of the satellite image to a map projection are derived. Explicit relations between the global accuracy of the transformation and the number, location, and local accuracy of the ground control points are obtained. The results are applied to the correction of a Landsat MSS image.

INTRODUCTION

THE QUANTITATIVE USE of remote sensing satellite images in many applications requires that the geometric distortion inherent in these images be corrected, or rectified, to a desired map projection. Rectification is necessary when the output products of image analysis are to be overlayed on a map or merged into a geographic data base. The most widely used rectification technique relies on the use of ground control points (GCPs) located in the image and the corresponding map in order to empirically determine a mathematical coordinate transformation to correct the geometry.

It is generally accepted that the number, location accuracy, and spatial distribution of GCPs influence the accuracy of the correction, but a quantitative analysis has not been reported in the literature. Bernstein (1976) presented a graph of the root-mean-square GCP error as a function of the number and accuracy of GCPs used, but did not publish the analysis leading to the graph. Ford *et al.* (1978) showed that the GCP mean-squared error is proportional to the image GCP error variance and the degree of the transformation polynomial, and inversely proportional to the number of GCPs. Forster (1980) reported residual errors for a correction example using 100 GCPs. The optimal distribution of GCPs is generally thought to be uniform over the entire image. This optimal distribution has been analyzed by Orti (1981) for an analytic correction of Landsat MSS images.

In this paper, we interpret the problem of geometric correction within the context of the general method of least squares by developing a statistical model of the transformation. Using known results from the method of least squares and derivations based on the model, we obtain expressions for the transformation coefficients and for the accuracy of the geometric transformation using these coefficients. The reliability of the transformation is analyzed and the error at every point in the map space is then estimated and expressed quantitatively as a function of the number, location, and measurement uncertainty of a specific set of GCPs. To provide guidance in the choice of a set of GCPs to achieve a desired transformation accuracy, statistical models for the spatial distribution of GCPs are developed, and expressions for the estimated error in the transformation are derived from this model. An example of application of the methodology to the geometric correction of a Landsat MSS subimage is presented and discussed.

REVIEW AND DISCUSSION OF GEOMETRIC CORRECTION

The geometric distortion of satellite images is due to the combined effects of the platform, the sensor operation, the scene, and the geometry of the map projection being referenced. The principal sources of distortion and estimates of the degree of compensation required for each have been described for Landsat MSS images (Bernstein, 1976; Van Wie and Stein, 1977). There are two general approaches to the rectification of this distortion: analytic correction and least-squares transformation. The analytic approach is based on a mathematical model of the image formation that results from the relative geometrical configuration of the scene, the platform,

PHOTOGRAMMETRIC ENGINEERING AND REMOTE SENSING,
Vol. 51, No. 11, November 1985, pp. 1725-1734.

0099-1112/85/5111-1725$02.25/0
© 1985 American Society for Photogrammetry and Remote Sensing

and the sensor. The parameters of this model are calculated from orbital data or are estimated from information in the acquired image, as described for Landsat MSS images by Horn and Woodham (1979) and Sawada (1981). This approach often does not provide correction at the desired level of accuracy, due to inadequacies of the model, to errors in the estimation of model parameters, and to unmodeled random distortion.

In the least-squares transformation approach, the image distortion is modeled empirically as a mapping transformation from the desired map projection coordinates to the acquired image coordinates. The mapping function is generally chosen to be a bivariate polynomial, first employed by Markarian *et al.* (1973). Denoting the map coordinates by (x_1,x_2) and the image coordinates by (y_1,y_2), the mapping functions are given by

$$y_1 = f_1(x_1,x_2) = \sum_{j=0}^{q} \sum_{k=0}^{q-j} a_{jk} x_1^j x_2^k \qquad (1)$$

$$y_2 = f_2(x_1,x_2) = \sum_{j=0}^{q} \sum_{k=0}^{q-j} b_{jk} x_1^j x_2^k \qquad (2)$$

where q is the degree of the polynomial and $\{a_{jk}\}$ and $\{b_{jk}\}$ are unknown transformation coefficients. The choice of q is dependent on the degree of nonlinearity of the distortion. The degree q must be large to correct highly localized distortion, at the expense of an increase in the sensitivity to modeling errors. In recognition of this problem, Yao (1973) proposed a correction algorithm employing a series of piecewise biquadratic mappings constrained such that a smooth approximation could be obtained over the entire image.

The transformation coefficients are determined from a set of GCPs, which are physical features that can be accurately located in the image and on a corresponding map. Typical GCPs are highway intersections, airports, land-water interfaces, or field boundaries located with the aid of an interactive display or printer output in the form of shade prints (Van Wie and Stein, 1976; Forster, 1980) or enhanced curvilinear features (Ford *et al.*, 1983). Automated location techniques include the sequential similarity detection algorithm (Barnea and Silverman, 1972), adapted for use on Landsat images (Bernstein, 1976; Kaneko, 1976), and an edge correlation method (Van Wie and Stein, 1976).

The transformation coefficients are chosen to minimize the sum of squared errors between the image GCPs and the transformed map GCPs. The estimation of the coefficients has been shown to be a problem in multiple regression (Ford *et al.*, 1978; Forster, 1980). The image geometry is corrected by defining a rectangular interpolation grid in the map coordinates and applying the mapping transformation to each grid point to locate the point in the image. In general, this location falls between pixels in the acquired image and some form of interpolation or resampling is required to determine the intensity in the corrected image. Interpolation methods employed include the nearest neighbor, bilinear interpolation (Bernstein, 1976), and cubic convolution (Rifman, 1973).

LEAST-SQUARES COORDINATE TRANSFORMATION

Geometric correction can be interpreted as a least-squares coordinate transformation problem, and the known results from the method of least squares can be applied to the problem. In this section, we briefly summarize the basic results from the least squares method, primarily to introduce our notation, which is a matrix form of the notation of Wolberg (1967). For derivations of the basic results, refer to the texts by Mikhail (1976) and Wolberg (1967).

It is assumed that the mapping of map coordinates to image coordinates is accurately modeled by the transformation of Equations 1 and 2, which can be expressed in the form

$$\mathbf{y}_j = \boldsymbol{\phi}^T(\mathbf{x})\boldsymbol{\alpha}_j \qquad j = 1,2 \qquad (3)$$

where $\boldsymbol{\phi}(\mathbf{x})$ is a $p \times 1$ vector of polynomial functions of the map coordinate vector $\mathbf{x}$, and $\boldsymbol{\alpha}_j$ is a $p \times 1$ vector of unknown coefficients. The $n \times 1$ vector of image GCP observations, $\mathbf{y}_j$, is assumed to be fixed but subject to measurement errors due to the limited image resolution and the resulting difficulty in locating the GCP features. The image GCP measurements are assumed to be statistically independent, so the $n \times n$ covariance matrix $\boldsymbol{\Sigma}_j$ will be diagonal. The variances of the measurement errors can be estimated when the GCPs are located. The uncertainty in the map GCP locations, $\mathbf{x}_i$, $i = 1, 2, \ldots, n$, is proportionally much less than the uncertainty in the image GCP locations, and will be assumed to be negligible.

The least-squares problem is to determine the estimated transformation coefficient vector, $\hat{\boldsymbol{\alpha}}_j$, that minimizes the weighted sum of the squares of the residuals

$$J_j = \mathbf{r}_j^T \mathbf{W}_j \mathbf{r}_j \qquad (4)$$

where $\mathbf{W}_j$ is the $n \times n$ weight matrix, taken to be the inverse of the image GCP covariance matrix, $\boldsymbol{\Sigma}_j^{-1}$; and $\mathbf{r}_j$ is the $n \times 1$ vector of residuals

$$\mathbf{r}_j = \mathbf{y}_j - \hat{\mathbf{y}}_j \qquad (5)$$

and $\hat{\mathbf{y}}_j$ is the estimated image GCP location vector.

Defining the $n \times p$ matrix of transformed observed map GCPs as $\boldsymbol{\Phi}$, where the ith row of $\boldsymbol{\Phi}$ is $\boldsymbol{\phi}^T(\mathbf{x}_i)$, the estimated image GCP location vector is

$$\hat{\mathbf{y}}_j = \mathbf{\Phi}\, \hat{\boldsymbol{\alpha}}_j. \tag{6}$$

This is a linear least-squares problem, where the estimated transformation coefficient vector is given by

$$\hat{\boldsymbol{\alpha}}_j = [\mathbf{\Phi}^T \mathbf{W}_j \mathbf{\Phi}]^{-1} \mathbf{\Phi}^T\, \mathbf{W}_j\, \mathbf{y}_j. \tag{7}$$

This result is similar to the expression given by Ford *et al.* (1978), except for the introduction of the weight matrix.

PRECISION OF THE TRANSFORMATION

In order to have confidence in the geometric correction provided by the transformation characterized by the least-square coefficient estimates, we need some information on the precision of this transformation. One indication of the precision of the transformation is given by the uncertainty in the coefficient estimate. An estimate of the covariance of the least-squares coefficient vector is

$$\mathbf{S}_{\hat{\alpha}_j} = [\mathbf{\Phi}^T \mathbf{W}_j \mathbf{\Phi}]^{-1}. \tag{8}$$

It is significant to note that this covariance is simply the inverse of the least-squares normal equation matrix, and is obtained computationally as the by-product of the evaluation of the coefficient estimate from Equation 7. This uncertainty is a function of the locations of the map GCPs through $\mathbf{\Phi}$ and the variances of the image GCP measurement errors through $\mathbf{W}_j$. If the uncertainty in a coefficient is of the same order of magnitude as the coefficient estimate, it is clear that this estimate has a low reliability, or a low level of significance. In this situation, the appropriateness of the transformation model of Equation 3 must be questioned.

The precision of the transformation can be evaluated from an estimate of the variance of the estimated value of the image coordinate y_j: i.e.,

$$s^2_{\hat{y}_j} = \mathrm{E}\{(\hat{y}_j - \overline{y}_j)^2\},$$

where $\mathrm{E}\{\cdot\}$ is the expectation operator and $\overline{y}_j$ is the mean: i.e.,

$$\overline{y}_j = \mathrm{E}\{\hat{y}_j\} = \mathrm{E}\{\boldsymbol{\phi}^T \hat{\boldsymbol{\alpha}}_j\} = \boldsymbol{\phi}^T \overline{\boldsymbol{\alpha}}_j.$$

Substituting the expression for the transformation in Equation 3 and the covariance of the coefficient estimate from Equation 7, we find

$$\begin{aligned} s^2_{\hat{y}_j} &= \mathrm{E}\{\boldsymbol{\phi}^T(\mathbf{x})(\hat{\boldsymbol{\alpha}}_j - \overline{\boldsymbol{\alpha}}_j)(\hat{\boldsymbol{\alpha}}_j - \overline{\boldsymbol{\alpha}}_j)^T\, \boldsymbol{\phi}(\mathbf{x})\} \\ &= \boldsymbol{\phi}^T(\mathbf{x}) \mathbf{S}_{\hat{\alpha}_j} \boldsymbol{\phi}(\mathbf{x}) \\ &= \boldsymbol{\phi}^T(\mathbf{x})[\mathbf{\Phi}^T \mathbf{W}_j \mathbf{\Phi}]^{-1} \boldsymbol{\phi}(\mathbf{x}). \end{aligned} \tag{9}$$

It is important to note that this expression provides an estimate of the error variance at any point in the map space for a specific set of GCP observations. The effect of the number, location, and accuracy of the GCPs appears solely through the matrices $\mathbf{\Phi}$ and $\mathbf{W}_j$. Equation 9 can be interpreted as an error surface in the map space, and some general properties of this surface can be inferred. Because the expression (Equation 9) is positive definite and is a polynomial form of fourth degree in $\mathbf{x}$ for a set of biquadratic mapping functions, we can infer that along any line in map space it can either have only one local minimum, or two local minima and a local maximum, as shown in Figure 1.

The "goodness of fit" of the transformation can be assessed from the weighted sums of squared residual error, J_1 and J_2. These sums have a chi-squared distribution with $n - p$ degrees of freedom, and the confidence region at a significance level α is

$$J_j < \chi^2_{\alpha,n-p}$$

where $\chi^2_{\alpha,n-p}$ is the value of the chi-square distribution at significance level α and $n - p$ degrees of freedom. For example, for $\alpha = 0.05$ and $n - p = 25$, $\chi^2_{\alpha,n-p}$ is 37.65. Thus, we expect $J_j/(n - p)$ to exceed 1.51 in 5 percent of all observations for which $n - p = 25$. If J_j is not within this confidence region, there is cause for concern about the choice of the transformation model.

MEAN SQUARED ERRORS

Two easily interpreted indicators of the precision of the transformation are the apparent and true mean squared errors discussed by Ford *et al.* (1978), which can be derived from the model by assuming that all of the image GCP observation error variances are equal. The apparent or residual mean squared error is

$$\overline{\epsilon^2_{A_j}} \triangleq \frac{1}{n}\, \mathbf{r}_j^T \mathbf{r}_j. \tag{10}$$

Under the assumption of equal error variances, the weight matrix becomes

$$\mathbf{W}_j = \frac{1}{\sigma_j^2}\, \mathbf{I},$$

Equation 4 reduces to

$$J_j = \frac{1}{\sigma_j^2}\, \mathbf{r}_j^T \mathbf{r}_j,$$

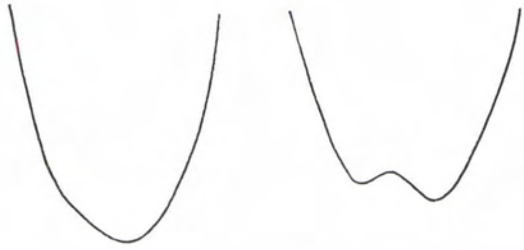

(a) (b)

FIG. 1. Possible forms of $s^2_{\hat{y}_j}$ along a line in map space.

TABLE 1. TRANSFORMATION OF GCPS—BIQUADRATIC

GCP No.	Observed Map GCPs Locations (UTM—kilometres)		Observed Image GCPs Locations (pixels)		Observed Image GCPs Std Devs (pixels)		Estimated Image GCPs Locations (pixels)		Residual Errors (pixels)	
i	x_{1i}	x_{2i}	y_{1i}	y_{2i}	σ_{1i}	σ_{2i}	$\hat{y}_{1i}$	$\hat{y}_{2i}$	r_{1i}	r_{2i}
1	624.980	3356.886	294.000	201.000	0.6	0.6	293.805	200.780	0.195	0.220
2	627.589	3355.405	344.000	213.000	0.6	0.6	344.680	213.343	−0.680	−0.343
3	628.398	3350.984	377.000	266.000	1.2	0.6	376.977	266.142	0.023	−0.142
4	633.590	3347.883	479.000	294.000	0.6	0.6	479.150	293.447	−0.150	0.553
5	622.463	3350.635	276.000	284.000	0.6	0.6	276.574	283.716	−0.574	0.284
6	621.798	3348.821	273.000	309.000	0.6	0.6	272.789	307.770	0.211	1.230
7	620.353	3352.262	233.000	269.000	0.6	0.6	233.545	268.434	−0.545	0.566
8	621.030	3354.198	237.000	242.000	0.6	0.6	237.115	242.879	−0.115	−0.879
9	618.165	3349.571	207.000	306.000	0.6	0.6	207.251	307.039	−0.251	−1.039
10	622.408	3360.630	235.000	161.000	0.6	0.6	234.373	160.386	0.627	0.614
11	624.914	3358.894	285.000	176.000	0.6	0.6	284.442	176.200	0.558	−0.200
12	628.091	3369.715	296.500	37.500	1.2	0.6	295.507	37.037	0.993	0.463
13	616.216	3368.711	96.000	76.000	0.6	0.6	95.775	75.197	0.225	0.803
14	634.502	3350.544	483.000	258.000	0.6	0.6	483.558	258.752	−0.558	−0.752
15	635.829	3351.756	501.000	241.000	0.6	0.6	501.233	241.158	−0.233	−0.158
16	621.638	3347.129	278.000	329.000	0.6	0.6	277.203	329.180	0.797	−0.180
17	627.301	3364.153	304.000	106.000	0.6	0.6	304.089	106.558	−0.089	−0.558
18	624.480	3368.220	239.000	63.000	0.6	0.6	239.487	62.816	−0.487	0.184
19	623.200	3369.640	212.000	48.000	0.6	0.6	211.926	48.222	0.074	−0.222
20	621.660	3367.360	195.000	79.000	0.6	0.6	194.523	79.449	0.477	−0.449
21	621.080	3367.670	183.000	77.000	0.6	0.6	183.345	76.937	−0.345	0.063
22	620.460	3371.310	158.000	33.000	0.6	0.6	158.372	33.798	−0.372	−0.798
23	634.950	3351.090	490.000	251.000	0.6	0.6	488.949	251.118	1.051	−0.118
24	627.638	3366.376	301.000	79.000	0.6	0.6	300.974	78.684	0.026	0.316
25	634.655	3356.809	460.000	182.000	0.6	0.6	460.098	181.459	−0.098	0.541

and the apparent mean squared error is

$$\overline{\epsilon^2_{A_j}} = \frac{J_j}{n}\,\sigma_j^2.$$

Because J_j is chi-square with $n - p$ degrees of freedom, it has an expected value of $n - p$ and we have

$$E\{\overline{\epsilon^2_{A_j}}\} = \frac{n-p}{n}\,\sigma_j^2. \tag{11}$$

The true mean squared error is

$$\overline{\epsilon^2_{T_j}} \triangleq \frac{1}{n}\,\|\boldsymbol{\Phi\alpha}_j - \hat{\mathbf{y}}_j\|^2 = \frac{1}{n}\,\|\boldsymbol{\Phi\alpha}_j - \mathbf{y}_j\|^2 - \overline{\epsilon^2_{A_j}},$$

and taking the expectation

$$E\{\overline{\epsilon^2_{T_j}}\} = \sigma_j^2 - \frac{n-p}{n}\,\sigma_j^2 = \frac{p}{n}\,\sigma_j^2. \tag{12}$$

Thus, as n increases, the apparent mean squared error at the GCPs approaches the variance of the image GCP observation error, and the true mean squared error falls off as $1/n$. Assuming a variance $\sigma_j^2 = 1$ (pixel^2) for the image GCPs, we see that to get the true mean squared error below 1/4 pixel (i.e., errors larger than 1 pixel with low probability), we require $n = 4p$, or more than 20 GCPs for $p = 6$. Note that the required number of GCPs is directly proportional to the number of coefficients to be determined.

EFFECTS OF THE GCP SPATIAL DISTRIBUTION

To achieve the geometric correction of an image at a desired level of accuracy, guidance in the choice of a set of GCPs is needed. While the expression for the uncertainty in the transformation of Equation 9 implicitly relates the error in the transformation to the number, location, and accuracy of a particular set of GCPs, it is difficult to interpret, because the effect of the GCPs enters through the matrices $\boldsymbol{\Phi}$ and $\mathbf{W}_j$. By developing and analyzing a model for the spatial distribution of the GCPs, we can gain greater insight on the effect of the GCPs on the accuracy of the transformation.

We now model the GCPs as spatially random vectors, instead of fixed locations. The map GCPs are assumed to be random samples of the independent variables x_1 and x_2. Two different spatial distributions are considered: Gaussian and uniform.

We will develop this model for a biquadratic transformation, where $p = 6$ and the vector transformation function is

TABLE 2. TRANSFORMATION VECTORS—BIQUADRATIC

	Coordinate y_1		Coordinate y_2	
k	Coefficients $\hat{\alpha}_{1k}$	Uncertainty $s_{\hat{\alpha}_{1k}}$	Coefficients $\hat{\alpha}_{2k}$	Uncertainty $s_{\hat{\alpha}_{2k}}$
1	296.987	2.56	182.649	2.47
2	17.1581	0.0298	−2.1809	0.0273
3	−4.0944	0.02169	−12.3050	0.0194
4	−0.000473	0.00571	0.0111	0.00537
5	0.006779	0.00311	0.004905	0.00294
6	−0.000753	0.00481	0.006848	0.00424

$$\boldsymbol{\phi}(\mathbf{x}) = \begin{vmatrix} 1 \\ x_1 - \bar{x}_1 \\ x_2 - \bar{x}_2 \\ (x_1 - \bar{x}_1)^2 \\ (x_2 - \bar{x}_2)^2 \\ (x_1 - \bar{x}_1)(x_2 - \bar{x}_2) \end{vmatrix} \tag{13}$$

where $(\bar{\cdot})$ denotes a sample average over the observed GCPs.

GAUSSIAN GCP SPATIAL DISTRIBUTION

If the GCPs are strongly localized in map space, they can be modeled as having a Gaussian spatial distribution. While this distribution is not commonly encountered in practice, it is analytically tractable and provides useful inferences. Assume that the map GCPs are random samples of the independent variables x_1 and x_2, where x_1 is Gaussian with mean $\bar{x}_1$ and variance $\sigma_{x_1}^2$ and x_2 is Gaussian with mean $\bar{x}_2$ and variance $\sigma_{x_2}^2$.

Under this assumption, the expected value of the least-squares normal equation matrix is

$$\begin{aligned}\langle \mathbf{N}_j \rangle &= \langle \boldsymbol{\Phi}^{\mathrm{T}} \mathbf{W}_j \boldsymbol{\Phi} \rangle \\ &= \operatorname{tr}(\mathbf{W}_j) \operatorname{diag}\,(1, \sigma_{x_1}^2, \sigma_{x_2}^2, 2\sigma_{x_1}^4, 2\sigma_{x_2}^4, \sigma_{x_1}^2\sigma_{x_2}^2)\end{aligned}$$

where $\langle \cdot \rangle$ denotes expectation with respect to $\mathbf{x}$ and tr is the trace operator. Because $\langle \mathbf{N}_j \rangle$ is diagonal, it is easily inverted and $\langle \mathbf{N}_j \rangle^{-1}$ is identical to $\langle \mathbf{N}_j^{-1} \rangle$. The expected value of the uncertainty in the transformation from Equation 9 for the Gaussian case is

$$\begin{aligned}\langle s_{\hat{y}_j}^2 \rangle_G &= \boldsymbol{\phi}^{\mathrm{T}}(\mathbf{x}) \, \langle \mathbf{N}_j \rangle^{-1} \boldsymbol{\phi}(\mathbf{x}) \\ &= [\operatorname{tr}(\mathbf{W}_j)]^{-1} \boldsymbol{\phi}^{\mathrm{T}}(x)[\operatorname{diag} \qquad (14) \\ &\quad (1, \sigma_{x_1}^{-2}, \sigma_{x_2}^{-2}, \tfrac{1}{2}\sigma_{x_1}^{-4}, \tfrac{1}{2}\sigma_{x_2}^{-4}, \sigma_{x_1}^{-2}\sigma_{x_2}^{-2}]\boldsymbol{\phi}(\mathbf{x}).\end{aligned}$$

Substituting the vector transformation function from Equation 13 and defining the centered, normalized coordinates

$$u_j = \frac{(x_j - \bar{x}_j)}{\sigma_{x_j}^2}, \; j = 1,2, \tag{15}$$

Equation 14 reduces to

$$\langle s_{\hat{y}_j}^2 \rangle_G = [\operatorname{tr}(\mathbf{W}_j)]^{-1}[1 + u_1^2 + u_2^2 + \frac{1}{2}(u_1^2 + u_2^2)^2].$$

Defining radius r in the normalized (u_1, u_2) map coordinates

$$r = (u_1^2 + u_2^2)^{1/2},$$

we have

$$\langle s_{\hat{y}_j}^2 \rangle_G = [\operatorname{tr}(\mathbf{W}_j)]^{-1}(1 + r^2 + \frac{1}{2} r^4). \tag{16}$$

This expression is easy to interpret. It indicates that the transformation variance is at a minimum at the map GCP sample average $(\bar{x}_1, \bar{x}_2)$, increases monotonically with the radius r, and is dominated by a term involving the fourth power of r for large r. If the image GCP observation error variances are equal, then

$$\operatorname{tr}(\mathbf{W}_j) = \operatorname{tr}(\boldsymbol{\Sigma}_j^{-1}) = \frac{n}{\sigma_j^2},$$

and the transformation variance is shown to be proportional to the common GCP error variance σ_j^2, and inversely proportional to the number of GCPs.

If a bilinear or affine transformation is an appropriate model of the distortion, Equation 16 becomes

$$\langle s_{\hat{y}_j}^2 \rangle_G = [\operatorname{tr}(\mathbf{W}_j)]^{-1}(1 + r^2). \tag{17}$$

It should be noted in this case that the error does not increase as rapidly with r as in the biquadratic case. This indicates that only the transformation having an order appropriate to the degree of the distortion should be applied, as higher order terms can only add uncertainty.

LOCALLY UNIFORM GCP SPATIAL DISTRIBUTION

In practical applications, the GCPs are often distributed nearly uniformly over a region in map space. Assuming that the map GCPs are random samples of the independent variables x_1 and x_2, and are uniformly distributed over a rectangle, then the density functions are given by

$$f_{x_j}(x_j) = \begin{cases} \dfrac{1}{x_{j1} - x_{j0}} & x_{j0} \le x_j \le x_{j1} \\ 0 & \text{otherwise,} \end{cases} \quad j = 1,2$$

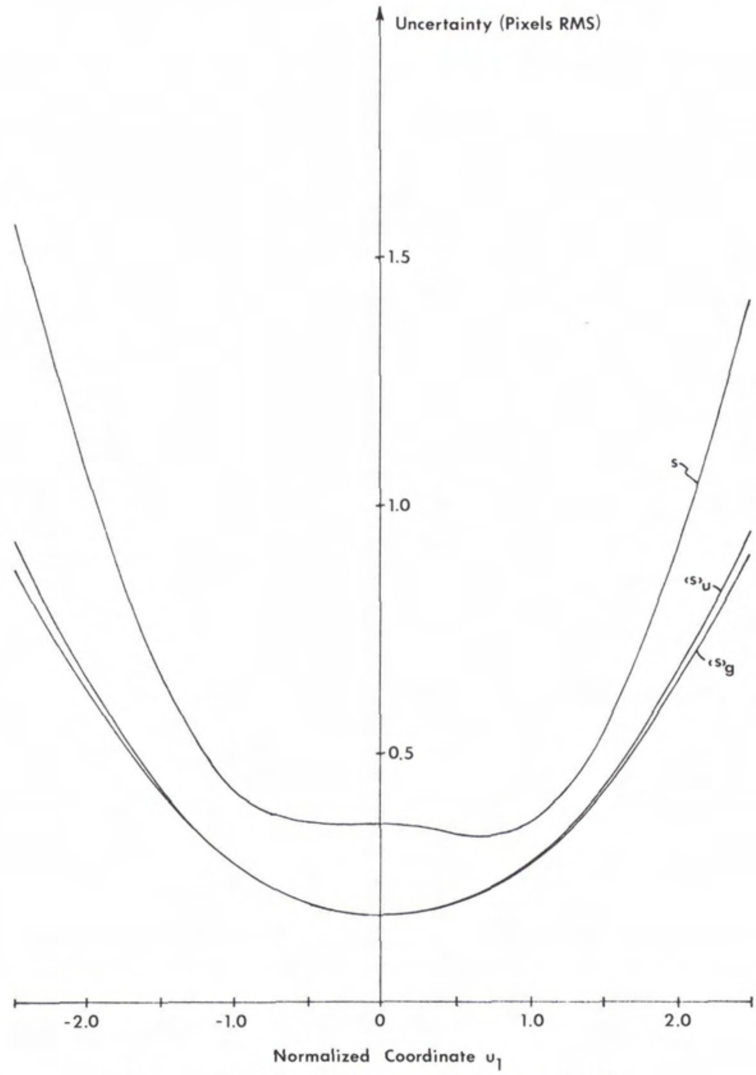

FIG. 2. Transformation uncertainty—biquadratic.

leading to the moments

$$\bar{x}_j = \frac{1}{2}(x_{j0} + x_{j1})$$

$$\sigma^2_{x_j} = \frac{1}{12}(x_{j1} - x_{j0})^2$$

and the expected value of the least-squares normal equation matrix is again found to be diagonal: i.e.,

$$\langle \mathbf{N}_j \rangle = \mathrm{tr}(\mathbf{W}_j)\ \mathrm{diag}(1, \sigma^2_{x_1}, \sigma^2_{x_2}, \frac{9}{5}\sigma^2_{x_1}, \frac{9}{5}\sigma^2_{x_2}, \sigma^2_{x_1}\sigma^2_{x_2}).$$

Using the normalized coordinates from Equation 15, the expected value of the uncertainty in the transformation for the uniform case is

$$\langle s^2_{\hat{y}_j} \rangle_U = [\mathrm{tr}(\mathbf{W}_j)]^{-1} \left[1 + u_1^2 + u_2^2 + \frac{5}{9}u_1^4 + u_1^2u_2^2 + \frac{5}{9}u_2^4\right].$$

This expression cannot be written in terms of the normalized radius r alone. However, defining the normalized polar coordinates

$$u_1 = r\cos\theta$$
$$u_2 = r\sin\theta,$$

the expression becomes

$$\langle s^2_{\hat{y}_j} \rangle_U = [\mathrm{tr}(\mathbf{W}_j)]^{-1} \left[1 + r^2 + \frac{5}{9}r^4 - \frac{1}{72}r^4(1 - \cos 4\theta)\right] \tag{18}$$

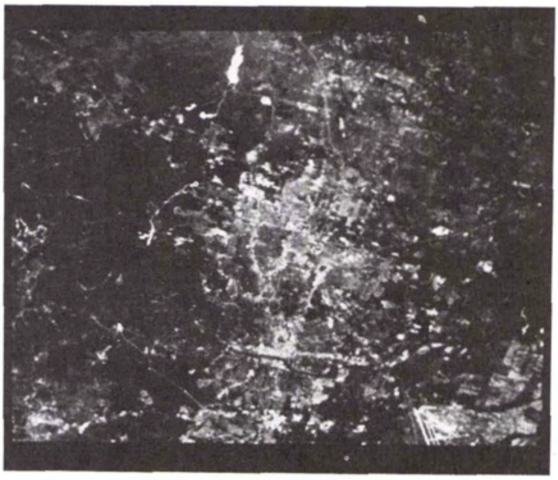

FIG. 3. Original Landsat band 4 subimage of Austin, Texas.

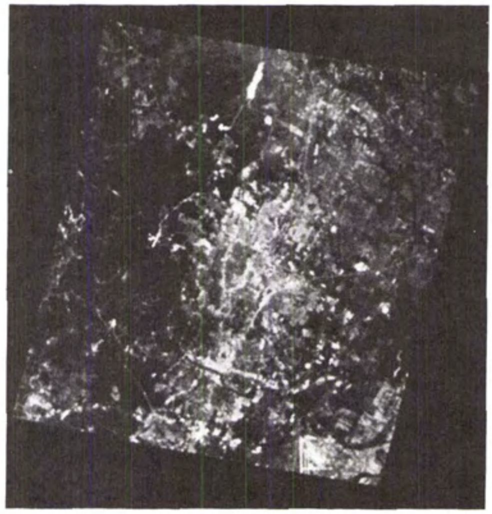

FIG. 4. Geometrically corrected Landsat subimage.

The error distribution is slightly anisotropic with a minimum for $\cos 4\theta = -1$ or $\theta = \pi/4 + k\pi/2$. Along the normalized coordinate axes ($\theta = 0$ or $\pi/2$), this reduces to

$$\langle s^2_{\hat{y}j} \rangle_U = [\mathrm{tr}(\mathbf{W}_j)]^{-1}(1 + r^2 + \frac{5}{9} r^4),$$

which is very similar to the result given in Equation 16 for the Gaussian GCP spatial distribution, the only difference being the slightly larger coefficient of the r^4 term in the uniform case.

Comparing results for the Gaussian and uniform spatial GCP distributions, we can conclude that the error in the transformation is not strongly influenced by the form of the spatial GCP distribution, but is controlled by the number and spatial variances of the GCPs. To minimize transformation errors, GCPs should be selected so that the spatial variances are large.

APPLICATION TO LANDSAT MSS DATA

We have applied the results obtained to the geometric correction of a Landsat MSS subimage near Austin, Texas. We applied the biquadratic transformation ($p = 6$), using the mapping functions of Equation 13, and compared it to the affine transformation ($p = 3$), which Horn and Woodham (1979) have shown to be an appropriate transformation for Landsat subimages if small, second order effects are neglected.

Using line printer output of enhanced curvilinear features from bands 5 and 7 (Ford *et al.*, 1983), 25 GCPs were acquired from the 410 by 512 pixel Landsat subimage, as listed in Table 1. We have found that GCPs can be located with this method with an error standard deviation of 0.6 pixels. For GCPs that are more difficult to locate, we assign a larger estimate of error standard deviation, as was done for GCPs number 3 and 12 listed in Table 1. The map GCP locations given in Table 1 are in UTM coordinates in kilometres, acquired from USGS topographic maps ($7^1/_2$ minute series) using a digital tablet.

For the biquadratic transformation, the coefficient vector computed from Equation 7 is given in Table 2. The estimated image GCP vectors, $\hat{\mathbf{y}}_j$, from Equation 6, and the residual vectors, $\mathbf{r}_j$, from Equation 5 are given in Table 1.

The residual errors are used to detect gross errors in the acquisition of GCP locations. If a residual is

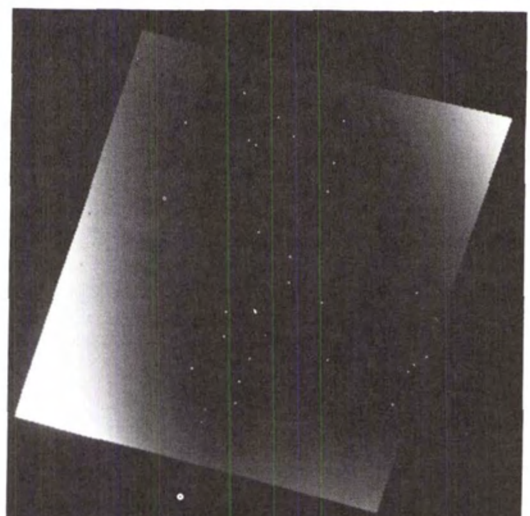

FIG. 5. Transformation uncertainty and GCPs displayed as an error surface image.

greater than three times the corresponding error standard deviation, that is, if

$$|r_{ji}| > 3\sigma_{ji},$$

then that GCP is considered as "suspect," and is examined to determine if an error was made in determining its location in the image or map. Graphics overlays on the image, showing the observed and estimated image GCP locations, are helpful in determining errors. As in all statistical problems, care must be taken in all decisions to remove outliers. All prior knowledge, such as alteration of GCP features from new construction or terrain induced distortion, must be taken into consideration in these decisions. These problems were not present in the example, as the residuals were all within two standard deviations.

The goodness of fit of the transformation is then considered. The weighted sums of square errors per degree of freedom for the example are

$$J_1/(n - p) = 0.749$$
$$J_2/(n - p) = 1.141,$$

which pass the chi-squared test at a 0.05 significance level, indicating a good fit. However, the uncertainties of the coefficients, $\mathbf{S}_{\hat{\alpha}_j}$ from Equation 8 given in Table 2 indicate some problems. Note that the uncertainties of the quadratic coefficients ($k = 3,4,5$) are of the same order of magnitude as the coefficients. This indicates that we have little confidence in the quadratic coefficients and that we would obtain better results from a bilinear or afine transformation.

To assess the accuracy of the transformation, we define the total transformation uncertainty as

$$s = (s^2_{\hat{y}_1} + s^2_{\hat{y}_2})^{1/2}, \tag{19}$$

where $s^2_{\hat{y}_j}$, $j = 1,2$, is given by Equation 9. Equivalent definitions can be made for $\langle s \rangle_G$ from Equation 16 for the Gaussian GCP spatial distribution model and for $\langle s \rangle_U$ from Equation 18 for the uniform GCP model. These uncertainties are plotted along the horizontal line through the origin in the normalized coordinates of Equation 15 ($u_2 = 0$) in Figure 2. Note that s does have two local minima as was suggested in Figure 1. The actual uncertainty, s, is greater than the estimated uncertainties ($\langle s \rangle_G$ and $\langle s \rangle_U$) because of the contributions of the off-diagonal terms of $[\mathbf{\Phi}^T \mathbf{W}_j \mathbf{\Phi}]^{-1}$.

The original Landsat subimage (band 4) is shown in Figure 3, and the corrected image, using the transformation from Table 2 and bilinear interpola-

TABLE 3. TRANSFORMATION OF GCPs—BILINEAR

GCP No.	Observed Map GCPs Locations (UTM—kilometres)		Observed Image GCPs Locations (pixels)		Observed Image GCPs Std Devs (pixels)		Estimated Image GCPs Locations (pixels		Residual Errors (pixels)	
i	x_{1i}	x_{2i}	y_{1i}	y_{2i}	σ_{1i}	σ_{2i}	$\hat{y}_{1i}$	$\hat{y}_{2i}$	r_{1i}	r_{2i}
1	624.980	3356.886	294.000	201.000	0.6	0.6	294.212	201.346	−0.212	−0.346
2	627.589	3355.405	344.000	213.000	0.6	0.6	344.997	213.886	−0.997	−0.886
3	628.398	3350.984	377.000	266.000	1.2	0.6	376.920	266.575	0.080	−0.575
4	633.590	3347.883	479.000	294.000	0.6	0.6	478.610	293.425	0.390	0.575
5	622.463	3350.635	276.000	284.000	0.6	0.6	276.573	283.840	−0.573	0.160
6	621.798	3348.821	273.000	309.000	0.6	0.6	272.575	307.637	0.425	1.363
7	620.353	3352.262	233.000	269.000	0.6	0.6	233.749	268.411	−0.749	0.589
8	621.030	3354.198	237.000	242.000	0.6	0.6	237.454	243.085	−0.454	−1.085
9	618.165	3349.571	207.000	306.000	0.6	0.6	207.215	306.337	−0.215	−0.337
10	622.408	3360.630	235.000	161.000	0.6	0.6	234.824	160.850	0.176	0.150
11	624.914	3358.894	285.000	176.000	0.6	0.6	284.883	176.756	0.117	−0.756
12	628.091	3369.715	296.500	37.500	1.2	0.6	295.182	36.528	1.318	0.972
13	616.216	3368.711	96.000	76.000	0.6	0.6	95.653	74.843	0.347	1.157
14	634.502	3350.544	483.000	258.000	0.6	0.6	483.385	258.657	−0.385	−0.657
15	635.829	3351.756	501.000	241.000	0.6	0.6	501.191	240.827	−0.191	0.173
16	621.638	3347.129	278.000	329.000	0.6	0.6	276.740	328.829	1.260	0.171
17	627.301	3364.153	304.000	106.000	0.6	0.6	304.344	106.763	−0.344	−0.763
18	624.480	3368.220	239.000	63.000	0.6	0.6	239.366	62.834	−0.366	0.166
19	623.200	3369.640	212.000	48.000	0.6	0.6	211.620	48.141	0.380	−0.141
20	621.660	3367.360	195.000	79.000	0.6	0.6	194.520	79.586	0.480	−0.586
21	621.080	3367.670	183.000	77.000	0.6	0.6	183.310	77.038	−0.310	−0.038
22	620.460	3371.310	158.000	33.000	0.6	0.6	157.817	33.555	0.183	−0.555
23	634.950	3351.090	490.000	251.000	0.6	0.6	488.838	250.951	1.162	0.049
24	627.638	3366.376	301.000	79.000	0.6	0.6	301.047	78.647	−0.047	0.353
25	634.655	3356.809	460.000	182.000	0.6	0.6	460.431	181.153	−0.431	0.847

TABLE 4. TRANSFORMATION VECTORS—BILINEAR

	Coordinate y_1		Coordinate y_2	
k	Coefficients $\hat{\alpha}_{1k}$	Uncertainty $s_{\hat{\alpha}_{1k}}$	Coefficients $\hat{\alpha}_{2k}$	Uncertainty $s_{\hat{\alpha}_{2k}}$
1	297.417	0.123	183.213	0.120
2	17.1477	0.0233	−2.1850	0.0229
3	−4.0827	0.0164	−12.3173	0.0155

tion (Bernstein, 1976), is shown in Figure 4. The uncertainty in the transformation from Equation 19, and the map GCPs are shown as an error surface image in Figure 5, where higher intensity indicates larger uncertainties. The coordinates of Figure 5 are the same as those of Figure 4. Note how the map GCPs control the shape of the error surface.

For the bilinear or affine transformation, p is equal to 3 and the mapping functions of Equation 13 are applied for $k = 1,2,3$. The transformed GCPs are listed in Table 3 and the transformation coefficients are listed in Table 4. Note that the residuals are larger than in the biquadratic case, although they ae within three standard deviations. The weighted sums of squared errors per degree of freedom are

$$J_1/(n - p) = 0.907$$
$$J_2/(n - p) = 1.337,$$

which are again higher than for the biquadratic case, but still within the chi-squared confidence interval.

The uncertainty in the transformation along the line $u_2 = 0$ is shown in Figure 6. Note that these uncertainties are considerably below those shown in Figure 2 for the biquadratic transformation. The actual uncertainty s and the estimated uncertainty $\langle s \rangle$ are in close agreement as the off-diagonal terms of $[\mathbf{\Phi}^T \mathbf{W}_j \mathbf{\Phi}]^{-1}$ in Equation 9 do not contribute significantly to s in this case.

CONCLUSION

We have analyzed and quantified the errors in the least-squares transformation approach to geometric correction of satellite images. In particular, the estimated error in the transformation can be computed at every point in the map space for a specific set of GCPs. This is useful in a trial and error procedure for adding GCPs as a function of the number, location, and measurement errors of the GCPs to an initially selected set of GCPs. The statistical analysis of the transformation is useful in two ways. First, it shows that the error increases rapidly as a function of the distance from the GCP centroid. For a biquadratic transformation, the error is proportional to the fourth power of this distance. Secondly, it relates the error parameters to the region where GCPs are acquired and therefore provides guidance for the selection of a set of GCPs. An important conclusion is that the degree of the polynomial transformation must be determined from an analysis of the degree of the distortion in the image. Increasing the degree of the transformation results in a decrease in the residual errors between the

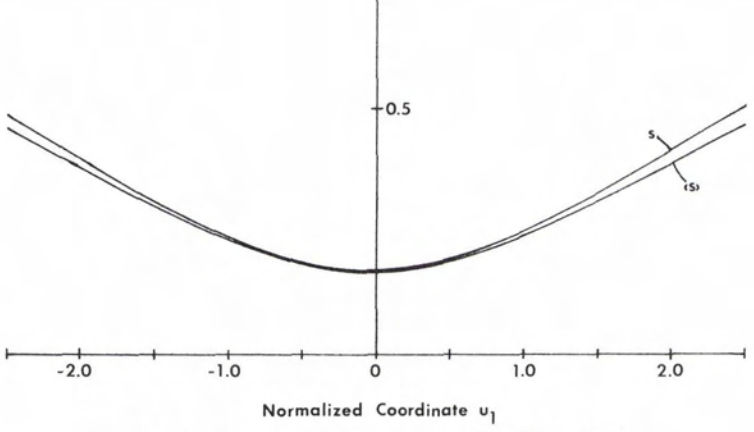

FIG. 6. Transformation uncertainty—bilinear.

observed and estimated GCPs, but does not necessarily decrease the actual errors between the observed and true GCPs, due to the uncertainties of the higher order coefficients.

ACKNOWLEDGMENT

This research was made possible in part through the funding of National Aeronautics and Space Administration under Grant NSG5092, and Contract NAS5-27577.

REFERENCES

Barnea, D. T., and H. Silverman, 1972. A Class of Algorithms for Fast Digital Image Registration, *IEEE Trans. on Computers*, Vol. C-21, pp. 179-186.

Bernstein, R., 1976. Digital Image Processing of Earth Observation Sensor Data, *IBM Journal of Research and Development*, Vol. 20, pp. 40-57.

Ford, G. E., V. R. Algazi, and B. G. Agee, 1978. On the Correction of Geometric Distortion in Satellite-Acquired Images, *Proceedings of the Twelfth Asilomar Conference on Circuits, Systems, and Computers*, pp. 341-344.

Ford, G. E., V. R. Algazi, and D. I. Meyer, 1983. A Non-Interactive Procedure for Land Use Determination, *Remote Sensing of Environment*, Vol. 13, No. 1, pp. 1-13.

Forster, B., 1980. Urban Control for Landsat Data, *Photogrammetric Engineering and Remote Sensing*, Vol. 46, pp. 539-545.

Horn, B. K. P., and R. J. Woodham, 1979. Landsat MSS Coordinate Transformations, *Proc. of 1979 Machine Processing of Remotely Sensed Data Symposium*, pp. 59-68.

Kaneko, T., 1976. Evaluation of LANDSAT Image Registration Accuracy, *Photogrammetric Engineering and Remote Sensing*, Vol. 42, pp. 1285-1299.

Markarian, H., R. Bernstein, D. G. Ferneyhough, L. E. Gregg, and F. S. Sharp, 1973. Digital Correction for High-Resolution Images, *Photogrammetric Engineering*, Vol. 39, pp. 1311-1320.

Mikhail, E. M., 1976. *Observations and Least Squares*, IEP, New York, 497 p.

Orti, F., 1981. Optimal Distribution of Control Points to Minimize Landsat Image Registration Errors, *Photogrammetric Engineering and Remote Sensing*, Vol. 47, pp. 101-110.

Rifman, S. S., 1973. Evaluation of Digitally Corrected ERTS Imagery, *Proceedings of the Symposium on Management and Utilization of Remote Sensing Data*, pp. 206-221.

Sawada, N., M. Kidode, H. Shinoda, H. Asada, M. Iwanaga, S. Watanabe, and K. Mori, 1981. An Analytic Correction Method for Satellite MSS Geometric Distortions, *Photogrammetric Engineering and Remote Sensing*, Vol. 47, pp. 1195-1203.

Van Wie, P., and M. Stein, 1977. A Landsat Digital Image Rectification System, *IEEE Trans. on Geoscience Electronics*, Vol. GE-15, pp. 130-137.

Yao, S. S., 1973. A Method for Digital Image Registration Using a Mathematical Programming Technique, *Proceedings of the Symposium on Machine Processing of Remotely Sensed Data*, pp. 1B-8 to 1B-23.

Wolberg, J. R., 1967. *Prediction Analysis*, D. Van Nostrand, Princeton, NJ, 291 p.

(Received 7 August 1982; revised and accepted 22 April 1985)

Forthcoming Articles

Paul S. Anderson, Millimetric Coordinates (MMC): Communication and Teaching Aid.
W. T. Borgeson, *R. M. Batson*, and *H. H. Kieffer*, Geometric Accuracy of Landsat-4 and Landsat-5 Thematic Mapper Images.
James K. Crossfield, A High Precision Photogrammetry Geodetic Positioning Cost Model.
V. Kratky, Software Simulation of On-Line Analytical Systems.
James E. Lee and *Steven D. Johnson*, Expectancy of Cloudless Photographic Days in the Contiguous United States.
G. D. Lodwick and *S. H. Paine*, A Digital Elevation Model of the Barnes Ice-Cap Derived from Landsat MSS Data.
William J. Ripple, Asymptotic Reflectance Characteristics of Grass Vegetation.
Alain Royer, *Pierre Vincent*, and *Ferdinand Bonn*, Evaluation and Correction of Viewing Angle Effects on Satellite Measurements of Bidirectional Reflectance.
John F. Watkins and *Hazel A. Morrow-Jones*, Small Area Population Estimates Using Aerial Photography.
T. H. Lee Williams, Implementing LESA on a Geographic Information System—A Case Study.